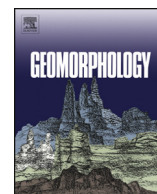




Contents lists available at ScienceDirect

# Geomorphology

journal homepage: [www.elsevier.com/locate/geomorph](http://www.elsevier.com/locate/geomorph)

## Origin and $^{10}\text{Be}$ surface exposure dating of a coarse debris accumulation in the Hrubý Jeseník Mountains, Central Europe

Zbyněk Engel <sup>a,\*</sup>, Régis Braucher <sup>b</sup>, Aster Team:

Georges Aumaître, Didier Bourlès, Karim Keddadouche

<sup>a</sup> Aix Marseille Univ., CNRS, IRD, Collège de France, INRAE, 13 545 Aix-en-Provence cedex 4, France<sup>a</sup> Charles University, Faculty of Science, Department of Physical Geography and Geocology, Albertov 6, 128 00 Praha, Czech Republic<sup>b</sup> Aix Marseille Univ., CNRS, IRD, Collège de France, INRAE, 13 545 Aix-en-Provence cedex 4, France

### ARTICLE INFO

#### Article history:

Received 11 May 2020

Received in revised form 31 May 2020

Accepted 31 May 2020

Available online 05 June 2020

#### Keywords:

Block slope

Surface exposure dating

Quaternary

Sudetes

### ABSTRACT

Coarse debris accumulations cover large areas in high latitude and mountain environments, but their age and origin remain mostly unknown. Here we reassess the morphology of a prominent coarse debris accumulation in the Sudetes Mountain range in central Europe and constrain its timing with  $^{10}\text{Be}$  surface exposure data. Our observations indicate that the landform in the south-eastern slope of the Sut' ridge appears consistent with the morphology of a block slope. The oldest minimum age of  $150.1 \pm 4.8$  ka obtained for the top at the upper limit of the block slope indicates the disintegration of the ridge and surface lowering under periglacial conditions prior to the last glacial-interglacial cycle. Four exposure ages retrieved for block samples range from  $84.3 \pm 3.8$  to  $26.8 \pm 2.6$  ka, providing evidence for block emplacement during the last cold period. The exposure ages extend existing chronological dataset for periglacial landforms in the Sudetes and constrain the timing of cold environments in the area prior the Last Glacial Maximum. The ages are also consistent with surface exposure data reported for block fields and block slopes in Western Europe and confirm the formation of similar landforms over the last glacial period in the Sudetes.

© 2020 Elsevier B.V. All rights reserved.

### 1. Introduction

Accumulations of coarse rock debris are characteristic features of periglacial domains in mountain and upland areas. They evolve either on low-angled ridges and plateaus as thin periglacial sheets with low relief or on steep valley sides where the deposits may assume different thicknesses and surface morphologies. Based on the plan form and morphological characteristics, block fields, block slopes, block streams, boulder lobes, debris flows, rock avalanche accumulations, rock glaciers and talus slopes are distinguished (Wilson et al., 2017). However, identification and classification of these landforms can be difficult, as their topography is highly variable and no quantitative characteristics are defined to discriminate these forms (van Steijn et al., 2002; Wilson, 2013). Periglacial block accumulations integrate a variety of transitional landforms that can be considered a continuum (Shakesby et al., 1987; Rea, 2013). The origin and age of these landforms are even more controversial, mainly due to poor chronological constraints (Rixhon and Demoulin, 2013). A major role in the evolution of autochthonous

block fields has been attributed to pre-Quaternary chemical weathering and/or frost action under cold conditions during the Quaternary (Ballantyne, 2010a). The nature of allochthonous block slopes or block streams remains poorly understood but most of these forms are considered to be relict (Wilson, 2013). Early attempts to date these features in Australia indicated their formation during the period of the maximum extension of glaciers in the last glacial (Last Glacial Maximum, LGM) but subsequent results of cosmogenic isotope surface exposure dating has assigned age of block streams and block slopes in other regions to pre-LGM cold stages (Table 1). By contrast, the formation of rock glaciers has been repeatedly associated with creep from interstitial ice or hydrostatic pressure during paraglacial phases (Janke et al., 2013; Knight et al., 2019). Other accumulations of coarse debris, controlled mainly by gravitational mass movements (rock avalanches, talus slopes and debris flows), also formed in paraglacial environments (Rixhon and Demoulin, 2013).

Several attempts have been made to establish the age of coarse debris accumulations but geochronological data are still rare. Some of the earliest attempts employed radiocarbon methods in the dating of relict block streams (Caine and Jennings, 1968). This approach focused on the dating of organic matter in sediments beneath block streams

\* Corresponding author.

E-mail address: [engel@natur.cuni.cz](mailto:engel@natur.cuni.cz) (Z. Engel).

**Table 1**  
Geochronological data reported for coarse debris accumulations.

| Landform          | Age (ka)         | Method                             | Region  | Reference                                      |
|-------------------|------------------|------------------------------------|---|--|
| Block field/slope | 600–70           | <sup>10</sup> Be, <sup>26</sup> Al | Allegheny Plateau, NE Pennsylvania            | Denn et al. (2018)                             |
|                   | 498–22.1         | <sup>36</sup> Cl                   | Ben Lomond Plateau, Tasmania                  | Barrows et al. (2004)                          |
|                   | <313–90.4        | <sup>36</sup> Cl                   | Mt. Wellington, Tasmania                      | Barrows et al. (2004)                          |
|                   | 144–10.7         | <sup>10</sup> Be, <sup>26</sup> Al | Torngat and Kaumajet Mts., Labrador Peninsula | Marquette et al. (2004)                        |
|                   | 143–36           | <sup>10</sup> Be                   | Little Diomed Island, Bering Strait           | Gualtieri and Brigham-Grette (2001)            |
|                   | 108–36.7         | <sup>10</sup> Be, <sup>26</sup> Al | Appalachian Mts., Pennsylvania                | Del Vecchio et al. (2018)                      |
|                   | 83.1             | <sup>36</sup> Cl                   | Sierra de Guadarrama, Iberian Peninsula       | Palacios et al. (2012)                         |
|                   | >81.8–33.5       | <sup>10</sup> Be, <sup>26</sup> Al | Scandinavian Mts., Sweden                     | Goodfellow et al. (2014)                       |
|                   | >55              | <sup>10</sup> Be, <sup>26</sup> Al | Scandinavian Mts., Norway                     | Brook et al. (1996)                            |
|                   | 37.8–22.6        | <sup>10</sup> Be                   | Slievenamon mountain, S Ireland               | Ballantyne and Stone (2015)                    |
|                   | 33.9–1.4         | <sup>10</sup> Be                   | Southern French Alps                          | Cossart et al. (2008)                          |
|                   | 30.7–9.8         | <sup>10</sup> Be, <sup>26</sup> Al | Scandinavian Mts., Norway                     | Andersen et al. (2018)                         |
|                   | 20.8–16.3        | <sup>36</sup> Cl                   | Victorian Alps, SE Australia                  | Barrows et al. (2004)                          |
|                   | 731–42           | <sup>10</sup> Be, <sup>26</sup> Al | Falkland Islands                              | Wilson et al. (2008)                           |
|                   | 143              | <sup>36</sup> Cl                   | Appalachian Mts., West Virginia               | Creameens et al. (2005)                        |
|                   | 65.0–18.4        | <sup>10</sup> Be                   | Mt. Biseul, Korean Peninsula                  | Rhee et al. (2017)                             |
|                   | 56.9–43.5        | <sup>36</sup> Cl                   | Mt. Mudeung, Korean Peninsula                 | Oh et al. (2012)                               |
|                   | >54–16           | OSL                                | Falkland Islands                              | Hansom et al. (2008)                           |
|                   | 46.8–43.4        | <sup>10</sup> Be, <sup>26</sup> Al | Mt. Maneo, Korean Peninsula                   | Seong and Kim (2003)                           |
|                   | 35.2             | <sup>14</sup> C                    | Snowy Mts., SE Australia                      | Caine and Jennings (1968)                      |
| 22.7–17.2         | <sup>36</sup> Cl | Snowy Mts., SE Australia           | Barrows et al. (2004)                         |  |
| Rock glacier      | 19.0–9.7         | <sup>10</sup> Be                   | Cairngorm Mountains, Scotland                 | Ballantyne et al. (2009)                       |
|                   | 17.3–14.2        | <sup>36</sup> Cl                   | Lesser Caucasus, Turkey                       | Dede et al. (2017)                             |
|                   | 16.3–12.3        | <sup>10</sup> Be                   | Cantabrian Mts., Iberian Peninsula            | Rodríguez-Rodríguez et al. (2016, 2017)        |
|                   | 16.1–5.7         | <sup>10</sup> Be                   | Sierra de La Demanda, Iberian Peninsula       | Fernández-Fernández et al. (2017)              |
|                   | 14.9–8.6         | <sup>36</sup> Cl                   | Pyrenees, Iberian Peninsula                   | Palacios et al. (2015ab), Andrés et al. (2018) |
|                   | 14.2–9.7         | <sup>10</sup> Be                   | Taurus Range, Anatolian Peninsula             | Çiner et al. (2017)                            |
|                   | 13.4–11.4        | <sup>10</sup> Be                   | Western Tatra Mts., Slovakia                  | Engel et al. (2017)                            |
|                   | 13.1–6.3         | <sup>36</sup> Cl                   | Sierra Nevada, Iberian Peninsula              | Palacios et al. (2016)                         |
|                   | 12.9–9.2         | <sup>36</sup> Cl                   | European Alps, Austria                        | Moran et al. (2016)                            |
|                   | 12.6             | <sup>10</sup> Be                   | Mount Washington, New Hampshire               | Bierman et al. (2015)                          |
|                   | 11.8–10.4        | <sup>10</sup> Be                   | High Tatra Mts., Slovakia                     | Zasadni et al. (2020)                          |
|                   | 10.3             | <sup>14</sup> C                    | European Alps, Italy                          | Krainer et al. (2015)                          |
|                   | >8–3             | OSL, IRSL                          | European Alps, Switzerland                    | Fuchs et al. (2013)                            |
|                   | 6.8              | <sup>10</sup> Be                   | European Alps, Switzerland                    | Haeblerli et al. (2003)                        |
|                   | 6.3–5.6          | <sup>10</sup> Be                   | Pyrenees, Iberian Peninsula                   | Palacios et al. (2017)                         |
|                   | >2.2             | <sup>14</sup> C                    | Absaroka Mountains, Wyoming                   | Konrad et al. (1999)                           |
|                   | >2.2             | <sup>14</sup> C                    | European Alps, Italy                          | Calderoni et al. (1998)                        |
| >0.8              | <sup>14</sup> C  | European Alps, Switzerland         | Scapozza et al. (2010)                        |  |

providing a maximum age constraint for the dated landforms. Radiocarbon dating has been also applied on organic impurities in ice and debris layers drilled from rock glaciers (Calderoni et al., 1998; Haeblerli et al., 1999; Konrad et al., 1999; Scapozza et al., 2010; Krainer et al., 2015). Terrestrial *in situ* cosmogenic nuclide (TCN) dating has been frequently used to determine age of rock glaciers (Table 1) but it has also been employed to date block/boulder fields (Brook et al., 1996; Gualtieri and Brigham-Grette, 2001; Marquette et al., 2004; Palacios et al., 2012; Goodfellow et al., 2014; Ballantyne and Stone, 2015; Andersen et al., 2018; Del Vecchio et al., 2018; Denn et al., 2018), block slopes (Barrows et al., 2004), and block streams (Seong and Kim, 2003; Barrows et al., 2004; Creameens et al., 2005; Wilson et al., 2008; Oh et al., 2012; Rhee et al., 2017). Although the application of TCN in the dating of coarse debris deposits is complicated by the sporadic renewal of blocks (Marquette et al., 2004) and possibility of their complex exposure histories (Denn et al., 2018) it remains the most frequently used geochronological method in the field of periglacial geomorphology. Optically/infrared stimulated luminescence techniques have been used very rarely for the dating of coarse debris accumulations. The main reasons are the limited availability of fine sediments in dated landforms, variations in the luminescence signal between individual mineral grains, difficulties with the resetting of the luminescence signal prior to deposition, and saturation problems (Hansom et al., 2008; Fuchs et al., 2013).

Extensive but relatively thin coarse debris covers in the Sudetes have been interpreted as products of the strong physical disintegration of bedrock transformed by frost action under periglacial conditions during the Quaternary (Migoń, 1996, and references therein). Subsequent

studies have demonstrated that block fields and rock glaciers are inactive in the current climate and their evolution ceased before the onset of the Holocene (Leśniewicz, 1996; Żurawek, 1999). Coarse debris covers have been associated with repeated phases of frost action during cold periods (Traczyk and Migoń, 2000) and the last phase of their formation was tentatively synchronous with the Late glacial (Traczyk, 2004). The last glacial origin of a summit tor and one of ploughing blocks in the vicinity of an extensive block field in the West Sudetes has been confirmed based on TCN dating (Engel, 2007). <sup>10</sup>Be surface exposure data also constrained the timing of proglacial ramparts in this range that formed during the Late glacial (Engel et al., 2014). Nevertheless, the timing of block fields and block slopes has remained controversial due to the absence of direct chronological evidence.

In this study, we reassess morphology of a prominent debris accumulation in the East Sudetes mountain range, the central Europe, establish the timing of its formation and provide palaeoclimatic interpretation. The accumulation of coarse angular debris has been interpreted as a block field (Petránek, 1953) or relict rock glacier (Żurawek, 1999). Dated rock glaciers may provide information about the spatial and temporal distribution of permafrost (Haeblerli et al., 2006), glacier equilibrium line altitudes (Humlum, 1988), and a mean annual air temperature (MAAT) during their formation (Brazier et al., 1998). By contrast, the palaeoenvironmental significance of block fields is limited due to poor understanding of the conditions required for the formation of these landforms (van Steijn et al., 2002). If blocks were formed by frost weathering *in situ* then block fields indicate former severe periglacial (permafrost) conditions (Ballantyne, 1998). The

palaeoclimatic interpretation presented here reflects the origin of the investigated debris accumulation reassessed based on morphological analysis and surface exposure dating.

## 2. Regional setting

The Hrubý Jeseník is the highest section of the East Sudetes mountain range, which represent the eastern end of the central European uplands (Fig. 1, insert map). The range is built by a tonalitic to granitic Cadomian crystalline basement imbricated with metamorphosed Devonian volcano-sedimentary complexes (Janoušek et al., 2014). It consists of the Keprník and Desná Domes deeply dissected by river valleys. Narrow ridges with well-developed summit planation surfaces at 1300–1460 m above sea level (a.s.l.) form the divides and adjacent steep slopes extend down to steeply graded streams. The fluvial morphology dominates the relief of the range, which was only slightly transformed by Quaternary glaciations. The only well-developed cirque is incised into the south-eastern slope of the Vysoká hole ridge (1464 m a.s.l.) in the southern section of the Desná Dome.

Unlike glaciers, periglacial processes left strong fingerprint in the landscape. A variety of periglacial landforms is preserved on summit planation surfaces and large accumulations of coarse rock debris and solifluction lobes cover valley slopes (Křížek, 2016). The investigated accumulation is located in the south-eastern slope of the Sut' ridge that descends from the southern section of the Hrubý Jeseník main ridge to the north-east (Figs. 1, 2). This side ridge has a gentle inclined north-western slope and a steep slope on the south-eastern side. A broad, low-angled divide of the ridge is covered with large sorted polygons. Coarse debris deposits and adjacent hillsides in the south-eastern slope of the ridge exhibit no evidence of glacial erosion.

The study area is located in a transitional zone between areas dominated by the oceanic climate and the continental type regimes. The

MAAT ranges from 1.3 °C at the Praděd summit (1491 m a.s.l.) to approximately 5 °C at an elevation of 1100 m a.s.l. (Uxa et al., 2019). The mean annual precipitation exceeds ~1200 mm on summit planation surfaces and decreases to 700 mm at the eastern foothills (Daniel et al., 2009). Westerly winds with the mean velocity up to  $8.5 \text{ m} \cdot \text{s}^{-1}$  prevail within the range transporting snow from the summit plateaus to leeward slopes (Sobíšek, 2000).

## 3. Methods

### 3.1. Geomorphological mapping and block sampling

The boundary of the coarse debris accumulation, concave breaks of slopes on its surface, and rock scarps at upper limit were mapped in the field using handheld GPS with the root-mean-square horizontal accuracy 1–2 m. The limits of identified landforms were adjusted subsequently based on the Digital Terrain Model of the Czech Republic (DMR 5G) with total mean elevation error of 0.18 m and 0.30 m in a treeless and forested terrain, respectively (COSMC, 2016). This model was also used to construct cross-sections and downslope profiles across the block slope. The difference between the cross-sections and bedrock surface approximated from valley slopes allow us to roughly estimate the thickness of the accumulation. The size, declination and inclination of blocks was analysed at the head of the accumulation, in its middle section and close to the terminus. At three test sites, we recorded the size of each of the three orthogonal axes (*a*-, *b*- and *c*-axes) of 25 blocks with a tape measure. Using a compass clinometer, we measured the azimuth and inclination of the long axis of blocks.

We sampled the largest tor at convex break of slope above the western section of the coarse debris accumulation and four blocks in its upper part for *in situ*  $^{10}\text{Be}$  surface exposure dating (Fig. 3). We collected block samples from the most distinct surface elevation to increase the chance of sampling the original undisturbed surface. We sampled one of the proximal blocks (sample SU-2) at the foot of the highest section of a hillslope tor to constrain the timing of the last phase of block production and emplacement. We also collected samples from blocks in the central (SU-3) and terminal (SU-5) section of the elevation that should approximate average and the oldest age of deposits. Finally, we took one sample from the block deposits (SU-4) below this elevation to obtain exposure age for adjacent part of the investigated accumulation. We selected only blocks larger than 1 m generated by disintegration of bedrock outcrops and scarp faces which are considered to be least affected by prior exposure or disturbance after deposition (Barrows et al., 2004). The samples were collected from the upper surface to the depth of 3–4 cm using a chisel and a hammer. The characteristics of sample sites are given in Table 2.

### 3.2. $^{10}\text{Be}$ methodology

The samples were crushed, sieved and cleaned with a mixture of HCl and  $\text{H}_2\text{SiF}_6$ . The extraction method for  $^{10}\text{Be}$  ( $T_{1/2}$ :  $1.387 \pm 0.017$ )Ma; Chmeleff et al., 2010; Korschinek et al., 2010) involves isolation and purification of quartz and elimination of atmospheric  $^{10}\text{Be}$ . A weighed amount (~0.1 g) of a 3025 ppm solution of  $^9\text{Be}$  was added to the decontaminated quartz. Beryllium was subsequently separated from the solution by successive anionic and cationic resin extraction and precipitation. The final precipitates were dried and heated at 800 °C to obtain  $\text{BeO}$ , and finally mixed with niobium powder prior to the measurements, which were performed at the French Accelerator Mass Spectrometry (AMS) National Facility ASTER (CEREGE, Aix en Provence).

The beryllium data were calibrated directly against the STD-11 beryllium standard using a  $^{10}\text{Be}/^9\text{Be}$  ratio of  $1.191 \pm 0.013 \cdot 10^{-11}$  (Braucher et al., 2015). Age uncertainties include an external AMS uncertainty of 0.5%, blank correction and  $1\sigma$  uncertainties (Arnold et al., 2010). The  $^{10}\text{Be}/^9\text{Be}$  measured blank ratio associated to the samples

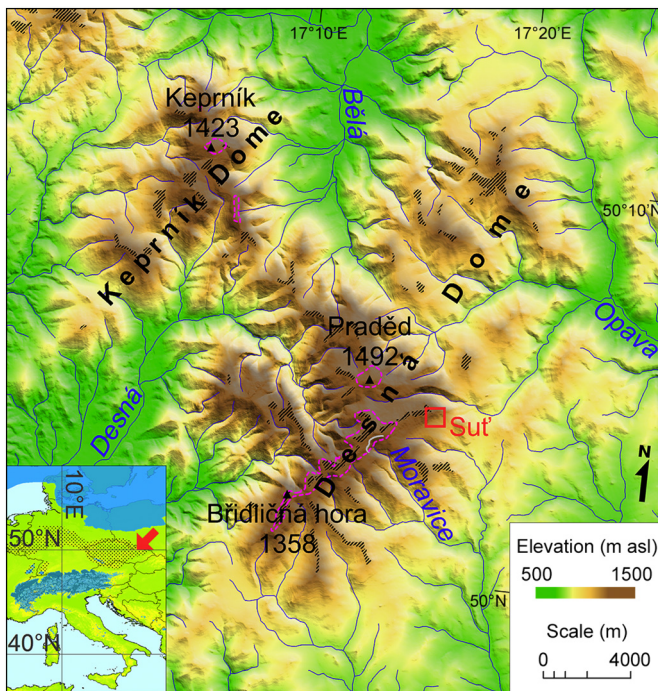


**Fig. 1.** Location of the study site in the Hrubý Jeseník Mountains and central Europe (inset). Oblique hatching marks planation surfaces, light grey line shows cirque closure of the Moravice valley and dashed purple line indicates the alpine timberline in the Hrubý Jeseník (after Tremil and Migoñ, 2015). Dotted area and blue shades in the insert map represent the central European uplands and LGM glaciation (after Ehlers et al., 2011), respectively. (For interpretation of the references to color in this figure legend, the reader is referred to the web version of this article.)

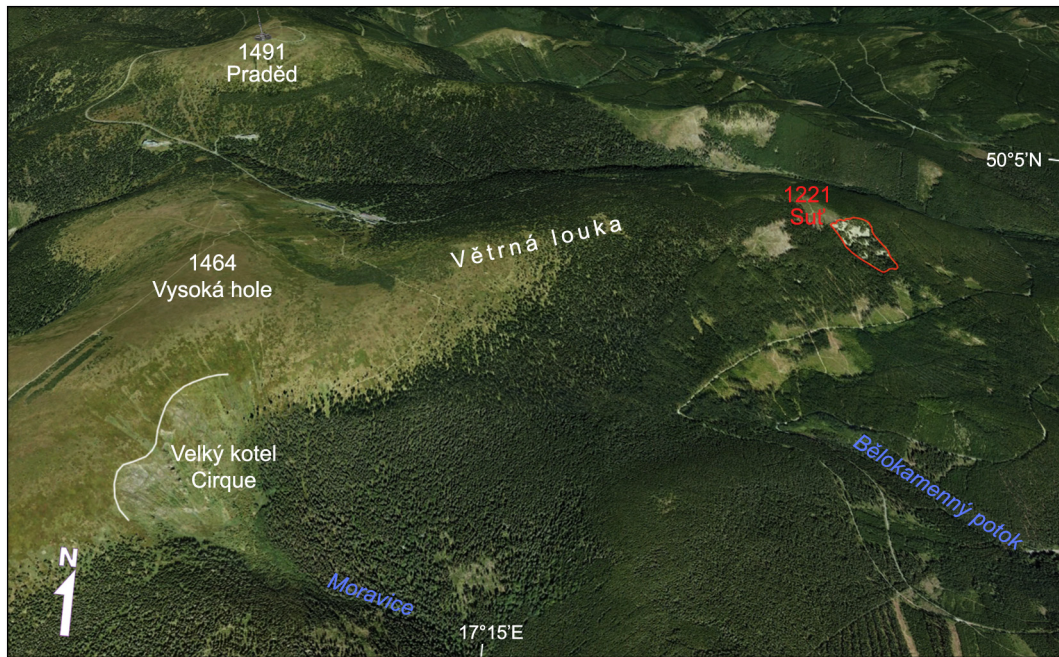


**Fig. 2.** Perspective view towards the investigated coarse debris accumulation (red line) from the south (Image credit: ©Google Earth). White line delimits glacial cirque in the upper Moravice valley. (For interpretation of the references to color in this figure legend, the reader is referred to the web version of this article.)

presented in this paper is  $3.618 \cdot 10^{-15}$ . A density of  $2.5 \text{ g} \cdot \text{cm}^{-3}$  was used for all samples. A sea-level, high-latitude spallation production of  $4.01 \pm 0.18 \text{ at g}^{-1} \cdot \text{yr}^{-1}$  (Borchers et al., 2016) was used and scaled

for latitude and elevation using Stone (2000) scaling scheme. The surface production rates were also corrected for the local slope and topographic shielding due to the surrounding terrain (Dunne et al., 1999).

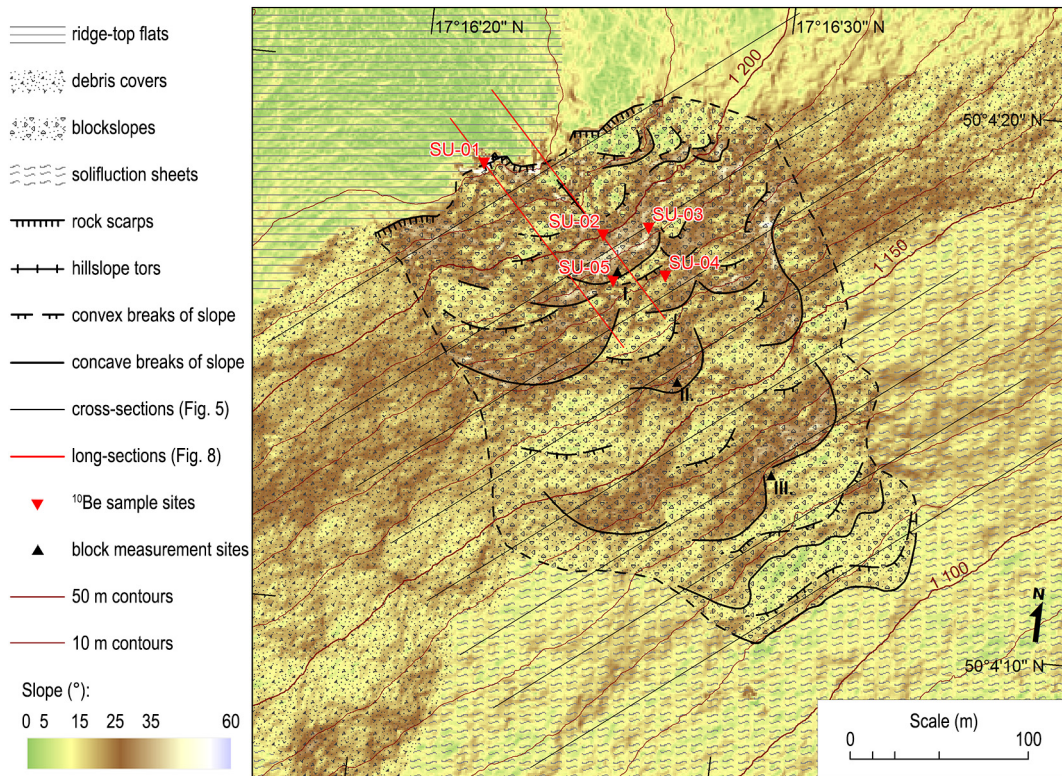


**Fig. 3.** Morphology of coarse debris accumulation with the location of block measurements (black triangles) and  $^{10}\text{Be}$  sample sites (red triangles). (For interpretation of the references to color in this figure legend, the reader is referred to the web version of this article.)

**Table 2**<sup>10</sup>Be sample site characteristics.

| Sample | Latitude (°N) | Longitude (°E) | Altitude (m a.s.l.) | Block length/width/height (m) | Sample thickness (cm) | Topographic shielding factor | Total shielding factor |
|--------|---------------|----------------|---------------------|-------------------------------|-----------------------|------------------------------|------------------------|
| SU-1   | 50.071717     | 17.272841      | 1220                | -*                            | 3                     | 0.999                        | 0.968                  |
| SU-2   | 50.071416     | 17.273820      | 1195                | 2.6/1.3/1.1                   | 3                     | 0.999                        | 0.96946                |
| SU-3   | 50.071473     | 17.274170      | 1188                | 3.6/2.7/1.7                   | 3                     | 0.999                        | 0.96855                |
| SU-4   | 50.071241     | 17.274337      | 1174                | 4.3/1.6/1.3                   | 4                     | 0.999                        | 0.96838                |
| SU-5   | 50.071192     | 17.273934      | 1179                | 4.9/3.1/1.8                   | 4                     | 0.997                        | 0.96746                |

\* Not relevant for bedrock sample.

Shielding from snow was estimated according to Gosse and Phillips (2001) using an average snow density of  $0.3 \text{ g}\cdot\text{cm}^{-3}$ , snow thickness of 40 cm and snow cover duration of 5 months at sample sites. These values were calculated based on measurements realized by the Czech Hydrometeorological Institute during the period 1961–2010 at six weather stations (550–1490 m a.s.l.) in the Hrubý Jeseník Mountains. However, as the variation in snow cover since the exposure of sampled surfaces is unknown, the true effect of snow shielding remains uncertain.

<sup>10</sup>Be concentrations were modelled using the equation:

$$C_{(x,\varepsilon,t)} = \frac{P_{spall}}{\Lambda_n + \lambda} \cdot e^{\frac{x}{\Lambda_n}} \left[ 1 - \exp\left\{-t\left(\frac{\varepsilon}{\Lambda_n} + \lambda\right)\right\} \right] + \frac{P_\mu}{\Lambda_\mu + \lambda} \cdot e^{\frac{x}{\Lambda_\mu}} \left[ 1 - \exp\left\{-t\left(\frac{\varepsilon}{\Lambda_\mu} + \lambda\right)\right\} \right] \quad (1)$$

where  $C_{(x,\varepsilon,t)}$  is the nuclide concentration as a function of depth  $x$  ( $\text{g}\cdot\text{cm}^{-2}$ ),  $\varepsilon$  the denudation rate ( $\text{g}\cdot\text{cm}^{-2}\cdot\text{yr}^{-1}$ ),  $t$  the exposure time (yr) and  $\lambda$  the radioactive decay constant ( $\text{yr}^{-1}$ ).  $P_{spall}$  and  $P_\mu$  are the relative production rates due to neutrons and muons, respectively.  $\Lambda_n$  and  $\Lambda_\mu$  are the effective apparent attenuation lengths ( $\text{g}\cdot\text{cm}^{-2}$ ), for neutrons and muons, respectively. The muon scheme follows Braucher et al. (2011).

To estimate minimum exposure ages, denudation was set to zero whereas the exposure time was supposed to be infinite to infer maximum denudation rates. In that latter case, it is possible estimating the time (integration time, noted  $T_{int.}$ ) needed to reach the steady state concentration using a modified equation based on the approach of Lal

(1991) which did not consider muon contributions; the modified equation is:

$$T_{int.} = \frac{\%P_{spall}}{\frac{\text{Ln}(2)}{1,387,000} + \frac{\varepsilon}{160}} + \frac{\%P_{\mu Slow}}{\frac{\text{Ln}(2)}{1,387,000} + \frac{\varepsilon}{1500}} + \frac{\%P_{\mu Fast}}{\frac{\text{Ln}(2)}{1,387,000} + \frac{\varepsilon}{4320}} \quad (2)$$

where  $\%P_{spall}$ ,  $\%P_{\mu Slow}$  and  $\%P_{\mu Fast}$  are the percentage contributions of neutrons, Slow and Fast muons respectively in the total production.

The distribution of the exposure ages obtained for four blocks and scatter in the age group were approximated using the reduced chi-square statistics ( $\chi^2_R$ ) and a standard deviation ( $1\sigma$ ) to the arithmetic mean exposure age ratio. The age group was classified following the procedure presented by Blomdin et al. (2016).

## 4. Results

### 4.1. Morphology of coarse debris accumulation

The investigated accumulation of coarse angular debris is located in the south-eastern slope of the Sut' ridge, covering  $0.057 \text{ km}^2$  of an upper valley-side slope area (Fig. 2). Spruce forest covers larger part of the accumulation and only  $0.013 \text{ km}^2$  of blocks in its upper part are exposed. The accumulation descends from the foot of a jointed bedrock scarp at 1220 m a.s.l. (Fig. 4) downslope to  $\sim 1105 \text{ m a.s.l.}$  A north-eastern (left) lateral part of the accumulation is clearly delimited against adjacent hillsides but its south-western side is characterized by a gradual transition to valley slope (Fig. 5A). Asymmetric cross-sections with convex-upward profiles in the upper part of the accumulation indicate a maximum thickness of debris cover deposits around 8–11 m. Transverse profiles in the terminal part are rather flat with highest sections raised only 2–3 m above adjacent hillsides. The terminus with a soil and lichen cover is slightly inclined and it merges gradually into footslopes. The length from the scarp to distal reaches attains 310 m, and the width ranges from 220 m in the upper part to 110 m at the terminus.

The upslope end of the accumulation is craggy in appearance as exposed bedrock scarp separates the upper part of debris slope from the plateau surface that stretches to the north (Fig. 3). The highly fractured scarp with occasional weathering pits on top surfaces is mostly 3–5 m high and it extends 80 m along the upper boundary of the debris accumulation. In the central section of the scarp, a narrow relict of the plateau stretches 35 m towards the south-east where it terminates with 7 m high rock face (Fig. 6). Upper part of the block slope below this hillslope top and adjacent sections of bedrock scarp is rugged in form with irregular pattern of distinctive rounded elevations (Fig. 3). Large, tongue-shaped elevations prevail in the upper parts of the debris accumulation above 1150 m a.s.l. whereas lobate downslope-arched forms perpendicular to the direction of movement extend between 1125 and 1110 m a.s.l. A step-like hillslope profile reflects the uneven surface of the accumulation which varies in angle from  $>40^\circ$  in downslope faces of the tongue-shaped elevations (Fig. 7A) to  $<20^\circ$  at their foot. Smooth, low-angled profiles follow up on footslopes beyond the terminus of coarse debris accumulation (Fig. 7B), where the downslope movement of debris produced gelifluction sheets. These evolved in the form of



**Fig. 4.** Sampled tor above the western section of coarse debris accumulation. Red arrow shows the sampled upper surface of the tor and red dots indicate a large block detached from the rock scarp. (For interpretation of the references to color in this figure legend, the reader is referred to the web version of this article.)

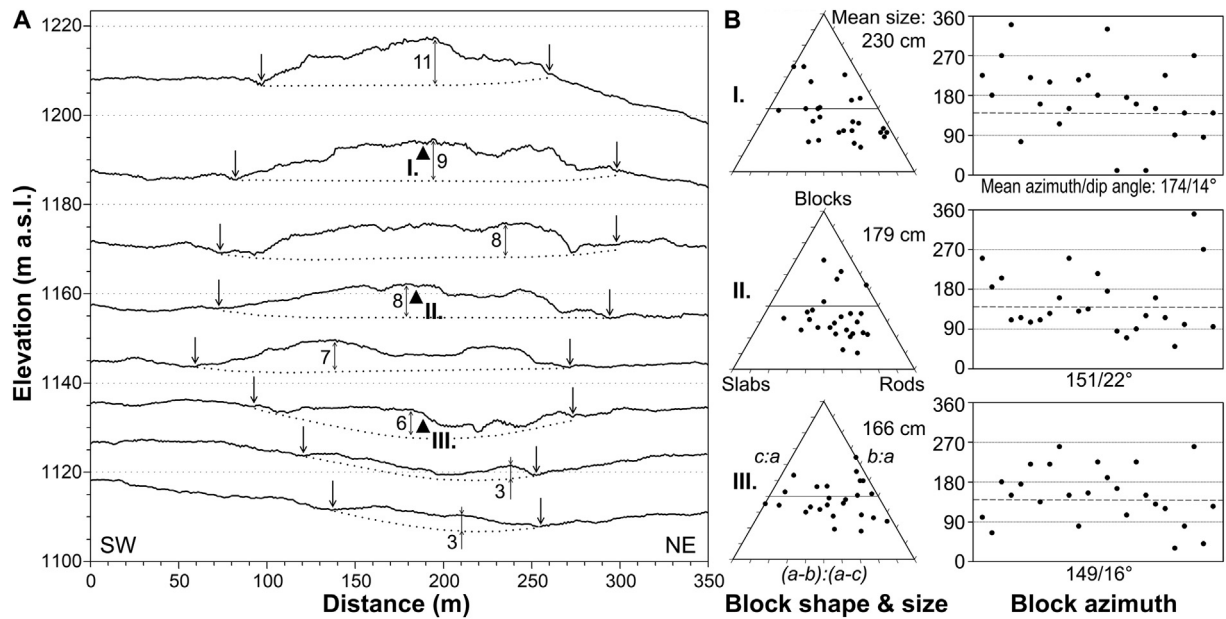


**Fig. 5.** Transverse profiles across the debris accumulation with indicated thickness estimate (meters) and location of block measurements (A). Block shape, size and declination for measured blocks (B). Triangular diagrams generated after [Graham and Midgley \(2000\)](#).

low elongated terraces and individual lobes that cover gentle slopes down to valley floors.

The coarse debris accumulation without a fine-grained matrix exhibits an openwork structure, the dominance of elongate and slab clasts, a downslope decrease in block size and downslope increase in orientation of blocks that are parallel with the local slope ([Fig. 5B](#)). The largest blocks with the *a*-axis up to 6.7 m long are located on upper slopes below the foot of bedrock scarp. The mean size of predominantly elongated blocks decreases from 2.3 m at an elevation above 1170 m a.s.l. to 1.7 m around 1110 m a.s.l. The downslope decrease in block size towards the terminus of debris accumulation differs from clast size distribution in adjacent gelifluction lobes and terraces, which exhibit the largest blocks at their front. Blocks on the surface of the accumulation are characterized by a marked downslope alignment along the mean slope aspect of 140°. The azimuth of the blocks at the head of the accumulation is highly variable and their mean angular difference from the slope aspect attains 34°. Moreover, only small part of blocks lies within 30° of the slope direction. Blocks in the lower part of the accumulation show a stronger preference for downslope orientation. A mean

difference of block azimuth from the aspect attains 11° in the middle section and 9° at the terminus. The transverse position of blocks and their imbrication is more frequent in downslope faces of both tongue-



**Fig. 6.** The upper part of coarse debris accumulation below the hillslope tor (behind trees in the middle of the horizon). Red arrow indicates 30 cm long hammer. (For interpretation of the references to color in this figure legend, the reader is referred to the web version of this article.)

**Fig. 7.** The downslope face of the largest surface elevation in the upper part of coarse debris accumulation (A) and slightly inclined front of this accumulation at 1110 m a.s.l. (B).

**Table 3**<sup>10</sup>Be surface minimum exposure ages, maximum denudation rates and corresponding integration times.

| Sample | Production rate (at <sup>-1</sup> g <sup>-1</sup> yr <sup>-1</sup> ) | <sup>10</sup> Be concentration (at <sup>-1</sup> g <sup>-1</sup> ) | <sup>10</sup> Be uncertainty | <sup>10</sup> Be Age (a) | Analytical / total uncertainty (± a) | Max. denudation rate (m/Ma) | Analytical / total uncertainty (± m/Ma) | Integration time (a) |
|--------|--|--|------------------------------|--------------------------|--------------------------------------|-----------------------------|---|----------------------|
| SU-1*  | 11.280   | 1,641,547  | 52,899                       | 150,089                  | 4837/7709                            | 4.32                        | 0.14/0.22                               | 139,887              |
| SU-2   | 11.040   | 295,487  | 28,484                       | 26,769                   | 2580/2794                            | 26.27                       | 2.53/2.74                               | 24,024               |
| SU-3   | 10.978   | 564,959  | 27,559                       | 51,791                   | 2526/3267                            | 13.28                       | 0.65/0.84                               | 48,617               |
| SU-4   | 10.786   | 896,578  | 39,890                       | 84,325                   | 3752/5045                            | 7.97                        | 0.35/0.48                               | 78,931               |
| SU-5   | 10.779   | 486,942  | 32,244                       | 45,389                   | 3006/3511                            | 15.24                       | 1.01/1.18                               | 41,929               |

\* Bedrock sample.

shaped and lobate surface elevations. Individual blocks at the margin of these surface forms have sub-vertical long axes.

#### 4.2. Surface exposure ages and steady-state denudation rates

The collected samples yield a large range in exposure age that span interval from ~150 to 27 ka (Table 3, Fig. 8). The oldest age of  $150.1 \pm 4.8$  ka was obtained for the outcrop (tor) sample SU-1 that is an order of magnitude older than the samples from blocks (Fig. 3). The oldest block age of  $84.3 \pm 3.8$  ka obtained (sample SU-4) is more than three times greater than the youngest block sample age of  $26.8 \pm 2.6$  ka and none of the four block sample age overlaps with the other samples within  $1\sigma$  uncertainties. This age group is poorly-clustered, because the block ages have a large scatter ( $\chi^2_R = 58$ ) and the standard deviation to the arithmetic mean exposure age ratio is 46%. This large scatter suggests that prior exposure or reactivation of individual sampled blocks after deposition must be considered in this age group. Considering the steady state scenario, the lowest denudation rate of  $4.32 \pm 0.14$  m/Ma was calculated for the tor (minimum integration time of 139.89 kyr) and values obtained for block samples range from  $7.97 \pm 0.35$  to  $26.27 \pm 2.53$  m/Ma. The corresponding minimum integration times are ranging from 78.93 to 24.02 kyr.

## 5. Discussion

### 5.1. Age and classification of coarse debris accumulation

The geomorphological evidence and surface exposure ages presented in this study suggest that frost action transformed the Sut' ridge over several cold periods but the accumulation of coarse debris in its south-eastern slope was probably formed during the last (Weichselian) glacial period. The exposure age of  $150.1 \pm 4.8$  ka obtained for the tor at the western section of bedrock scarp indicates disintegration of the south-eastern edge of the ridge during the penultimate (Saalian) glacial period. It should be noted that this interpretation relies on a single exposure age and needs to be treated with cautions. The tor represents the longest exposed surface on the Sut' ridge that is resistant to weathering or burial by sediments, and its disturbance since initial exposure is unlikely (Gunnell et al., 2013). On the other hand, cosmogenic-nuclide inheritance, another source of sampling uncertainties (Ballantyne, 2010b), cannot be excluded. Therefore, we consider the obtained exposure age may be apparently younger than the true age of the tor surface.

The sampled top of the tor has remained preserved since the Marine Isotope Stage (MIS) 6b but its south-eastern face has retreated and supplied blocks to downslope area over the next glacial-interglacial cycle. The distance of 35–50 m between the scarp and south-eastern tip of

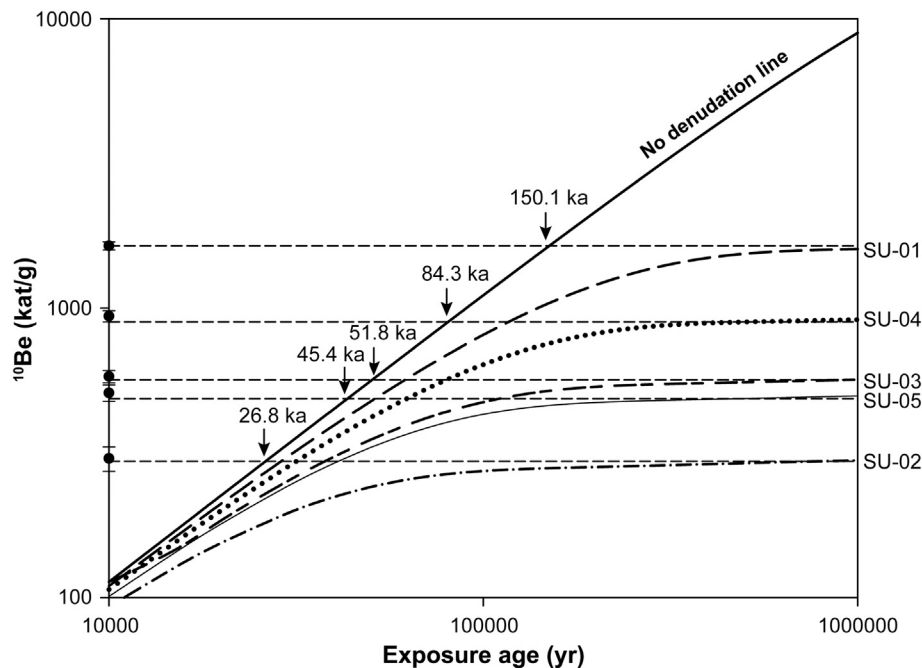


**Fig. 8.** Sample concentrations and minimum exposure ages. The horizontal dash lines refer to the sample concentrations. The No denudation line and the curves below represent the concentration evolution with time for sample exposed at surface with no denudation (black line), denudation of 4.32 m/Ma (long dash line corresponding to sample SU-1), denudation of 7.97 m/Ma (dotted line corresponding to sample SU-4), denudation of 13.28 m/Ma (long and medium dash line corresponding to sample SU-3), denudation of 15.24 m/Ma (thin black line corresponding to sample SU-5) and 26.27 m/Ma (dotted and dash line corresponding to sample SU-2). Minimum exposure ages of all samples are pointed by black arrows.

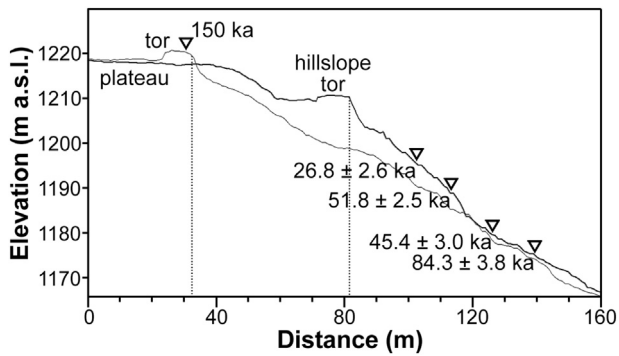


**Fig. 9.** Downslope profiles across the dated tor (thin line) and hillslope tor (bold line) in the upper part of the block slope with indicated location and exposure age of dated blocks. 1.5× vertical exaggeration.

the hillslope tor suggests that the scarp disintegrated into blocks rapidly under periglacial condition and retreated at a mean rate of  $\sim 0.2\text{--}0.3\text{ m}\cdot\text{ka}^{-1}$  (Fig. 9). This interpretation implies that scarp retreat and subsequent downslope transport of released blocks were the main processes that supplied material to the debris accumulation. The described evolution of blocks together with rapid retreat of the scarp reduces the possibility of significant initial exposure of blocks before their emplacement. By contrast, individual blocks could have slumped or toppled after emplacement that would result in younger age compared to other block ages. The postdepositional disturbance remains the most likely source of uncertainty within group of block ages and should be considered if the dataset is scattered (Balco, 2020).

The minimum surface exposure age of  $\sim 150\text{ ka}$  and the minimum integration time of  $140\text{ ka}$ , delimit the onset of block generation from the fractured scarp and bedrock outcrops representing the upper age bracketing for the exposure period of blocks. Thus it is logical that integration times retrieved for the sampled blocks are younger than this threshold. Further, a closer look at the location of the dated blocks (Fig. 9) reveals that the oldest and youngest blocks are emplaced in the lowest and highest elevation, respectively. An expected downslope increase in exposure ages cannot be confirmed because the block SU-5 ( $45.4 \pm 3.0\text{ ka}$ ) is younger than the up-slope block SU-3 ( $51.8 \pm 2.5\text{ ka}$ ). This may result from post-depositional toppling of the block SU-5 that is located below steep downslope face of the largest surface elevation in the upper part of the investigated accumulation. Regarding sample SU-4, the oldest sampled block, inheritance cannot be excluded but

it seems that the presence of Early to Late Weichselian ages in the dataset corresponds with chronology of many dated block streams/slopes and reflects long-term evolution of the accumulation over the last glacial period. In either case, the integration time of  $24.02\text{ ka}$  obtained for block SU-2 located at the foot of a hillslope tor represents a minimum age and may correspond to a final phase of frost-related block production and deposition. This interpretation confirms that the coarse debris accumulation in the south-eastern slope of the Sut' ridge is relict but it also rejects the hypothesis of the landform formation after ice retreat from the Hrubý Jeseník (Petránek, 1953).

The age estimates for block samples collected in the south-eastern slope of the Sut' ridge fall within the range of surface exposure ages reported for block fields and block slopes in mid-latitude regions including Europe (Table 1). The oldest age from the Sudetes coincides with a single exposure age of  $83.1 \pm 1.7\text{ ka}$  reported by Palacios et al. (2012) for a block field in the central part of the Iberian Peninsula. Almost the same exposure age of  $81.8 \pm 2.8\text{ ka}$  has been obtained by Goodfellow et al. (2014) for the oldest sampled block in the northern Scandinavian mountains where collected block field samples also reveal age range ( $81.8\text{--}33.5\text{ ka}$ ) that is similar to the Sudetes dataset. The timing of the youngest block emplacement in the study area corresponds with the phase of block field formation in southern Ireland ( $37.8\text{--}22.6\text{ ka}$ ; Ballantyne and Stone, 2015) and the southern Scandinavian mountains ( $30.7\text{--}9.8\text{ ka}$ ; Andersen et al., 2018). Our ages also confirm conclusions by Hopkinson and Ballantyne (2014) which attribute the age of blockfield debris on Scottish Mountains to the Late Pleistocene ( $<135\text{ ka}$ ). Three of four calculated ages indicate prevailing emplacement of blocks during warmer stages (MIS 5 and MIS 3) of the Weichselian (Fig. 10). This is in line with evidence of more efficient downslope transport of regolith in warm permafrost conditions (Matsuoka, 2001). Considering the exposure ages uncertainties, emplacement intervals started when NGRIP  $\delta^{18}\text{O}$  was low but increasing (grey curve on cyan shades in Fig. 10).

The integration age estimates reported here help to identify the origin of the investigated accumulation. This accumulation was initially described as a block field that served as a source of debris for poorly delimited rock glacier or solifluction lobe located downslope (Petránek, 1953). Subsequently, the landform has been interpreted as relict rock glaciers despite the lack of indicative morphological features (Žurawek, 1999). The morphological evidence reported here suggests that both two proposed hypotheses are incorrect. The location and surface gradient of the landform precludes its identification as a block field that represents a veneer of coarse regolith on upland plateaus or mountain summits with a gently sloping surface (Goodfellow, 2007). The

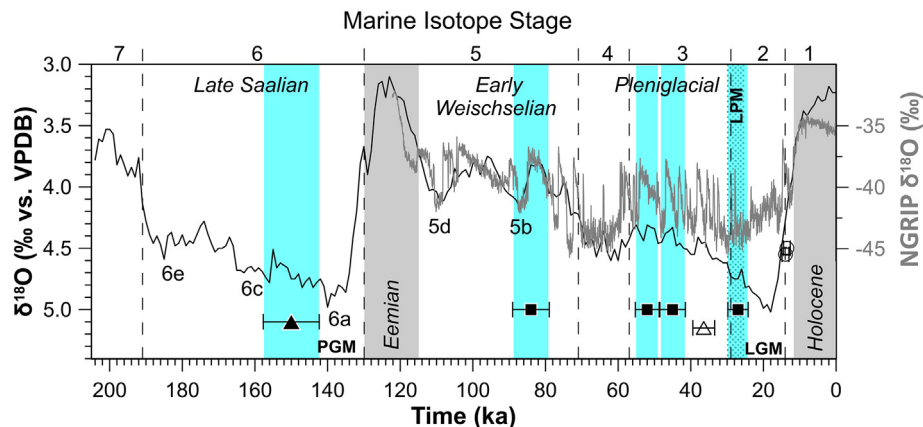


**Fig. 10.** Palaeoenvironmental constraints for evolution of slopes in the Sudetes since the penultimate glacial period. Full triangle and squares with bars and cyan shades represent single  $^{10}\text{Be}$  exposure ages with total uncertainty ranges for the dated tor and blocks, respectively. Empty triangle and circles show  $^{10}\text{Be}$  timing for a tor and protalus rampart in the West Sudetes (from Engel et al., 2014). The oxygen isotope data are from deep-sea (black curve) and ice (grey curve) cores from Lisiecki and Raymo (2005) and Rasmussen et al. (2014), respectively. Marine isotope stages and substages after Railsback et al. (2015), penultimate glacial maximum (PGM) after Colleoni et al. (2016), last permafrost maximum (LPM) after Andrieux et al. (2018) and last glacial maximum (LGM) after Clark et al. (2009). (For interpretation of the references to color in this figure legend, the reader is referred to the web version of this article.)

hillslope position and tongue-shaped planform of the landform are in line with morphological features of rock glaciers but other indicative characteristics (a concave upward profile near the head of the rock glacier and convex towards the toe, gradual transition from the source of debris input to the rock glacier, steep front slope near the angle of repose, transverse and longitudinal ridges and furrows) described by Janke et al. (2013) are missing. Moreover, the ages obtained for collected block samples are considerably older than dated rock glaciers that mostly formed after the LGM (Table 1). The ground plan of the investigated landform corresponds to a single-channelled type of block stream and block slope (Rixhon and Demoulin, 2013). Block streams may display open-work structure, downslope decrease in block size, and imbrication of blocks at lobate fronts, that were observed in the study area. But, most of these landforms occur on valley bottoms and display a concave-up longitudinal profile, elongated surface depressions or extensive longitudinal furrows, that are absent in the south-eastern slope of the Sut' ridge. Hence, the investigated landform may be interpreted as a block slope *sensu* van Steijn et al. (2002).

### 5.2. Palaeoenvironmental implications of block slope formation

The integration time of 140 ka associated with maximum denudation of  $4.32 \pm 0.14$  m/Ma obtained for the tor at the upper limit of the block slope indicates that surface lowering on the Sut' ridge *via* frost cracking and downslope transport of disintegrated bedrock occurred during the penultimate glacial period (Fig. 10). This period has been associated with intense frost weathering of tors and formation of debris slope cover in the northern Sudetic Foreland (Traczyk and Żurawek, 1999; Żurawek and Migoń, 1999). The development of these landforms in the later phase of MIS 6 reflects particularly cold and dry conditions in the Northern Hemisphere indicated by marine records, terrestrial proxies and climate simulations (Colleoni et al., 2016). However, there are no dated proxy records within the Sudetes that would confirm the occurrence of permafrost or enhanced periglacial activity in this period. Repeated intervals of periglacial activity (Traczyk and Migoń, 2000) and mountain glaciation (Carr et al., 2002; Sekyra and Sekyra, 2002) were tentatively associated with pre-Weichselian cold periods based on geomorphological and sedimentary evidence only. The denudation rate determined for the tor is well within the range of values reported for planation surfaces in mid-latitude uplands (Heimsath et al., 2010; Portenga et al., 2013; Crest et al., 2017) including the Sudetes (Danišik et al., 2010).

Periglacial modification of the Sut' ridge continued over the last cold period when frost-induced retreat of bedrock scarp and downslope transport of released block lead to the formation of the large block slope. The exposure age of 84 ka retrieved for the oldest dated block suggests that upper section of the block slope was exposed to cosmic rays since the beginning of the last glacial period (Early Weichselian). Following the temperature threshold reported by Harris (1994) for the formation of block streams, the MAAT was lower than  $-6$  °C. The climate was not as dry as during the LGM but it was sufficiently cold to enhance periglacial activity, aggradation of permafrost, and growth of ice sheets and mountain glaciations in central Europe (e.g., Svendsen et al., 2004; Žák et al., 2012; Andrieux et al., 2018). Although numerical data have been obtained on most complete sequences of moraines in the Sudetes, it is not clear if glaciers formed there during the Early Weichselian. Thermoluminescence dating has provided a chronological indication of pre-LGM glaciation but three ages centred at ~90 ka have been interpreted as time constraints for the penultimate (Saalian) glaciation (Chmal and Traczyk, 1999).  $^{10}\text{Be}$  exposure ages for the same moraines were reported as underestimated, and tentatively attributed to the interval ~36–21 ka (Engel et al., 2014). Hence, according to geomorphological and sedimentary evidence, the LGM glacier advance was preceded by a more extensive glaciation but its timing remains uncertain.

The two ages of block SU-3 and SU-5 fall into the first half of MIS 3 that started with rapid warming followed by large-amplitude climate

oscillations (Moseley et al., 2014; Agosta and Compagnucci, 2016). Considering the rapid climate changes during the intervals of exposure ages (Fig. 10), the MAAT threshold of  $-6$  °C applies only for short periods of time followed by prominent temperature increases. During the early MIS 3 warm phase, the air temperature was about  $6.3$  °C in the northern Sudetes forelands (Skrzypek et al., 2011), which is only  $2$  °C lower than the current MAAT. The warming enhanced the degradation of permafrost and formation of soils in lowland areas around the Sudetes (Žák et al., 2012; Antoine et al., 2013). At the elevations below 600–750 m a.s.l., stratified deposits formed as a result of shallow sheet solifluction (Traczyk, 1996). Loess sedimentation decreased and a vegetation mosaic of steppe, tundra scrubland, spruce and gallery forests developed (Feurdean et al., 2014; Lehmkuhl et al., 2016). As a result of the highly variable atmospheric circulation, warmer and more humid phases were repeatedly interrupted by cold and rather dry events (Van Meerbeek et al., 2011; Heiri et al., 2014). One of the coldest events culminated around 44 ka as evidenced by the ice-wedge formation across the central European loess belt (Antoine et al., 2016; Marks et al., 2019). The return to cold and dry periglacial environments started at the end of MIS 3 when permafrost aggraded, syngenetic ice-wedge casts formed and aeolian transport and sedimentation increased (Antoine et al., 2013; Woronko et al., 2015).

The youngest age of block SU-2 provides evidence for block slope activity at the onset of the MIS 2 (Fig. 10). At that time, cold and relatively wet conditions prevailed in the central European lowlands (Lehmkuhl et al., 2016), uplands (Alexandrowicz et al., 2013), and the Alpine region, where cooling and increase in moisture resulted in the largest expansion of glaciers over the Weichselian glacial period (Seguinot et al., 2018). Considering the uncertainty of the youngest sample age ( $26.8 \pm 2.6$  ka), the later phase of block slope activity falls within the period of the Last Permafrost Maximum in western Europe (30–24 ka, Andrieux et al., 2018). This phase also corresponds with the onset of the LGM glaciation in the West Sudetes where ice-free period terminated around 28 ka (Engel et al., 2014). In the Sudetes, the annual precipitation ranged from 500 to 700 mm during the LGM (Czudek, 2005) and the MAAT was estimated to vary between  $-8$  and  $-10$  °C at higher elevations (Chmal and Traczyk, 1993). Severe periglacial conditions dominated the mountain environments where continuous permafrost extended and reached its maximum thickness of 220–250 m (Czudek, 2005). The frost action ceased during the Lateglacial when the last period of enhanced periglacial conditions terminated (Traczyk, 2004). Forest, lichen and soil cover indicate recent stability of larger part of the block slope including its terminal section.

## 6. Conclusions

We have reassessed morphology of a prominent coarse debris accumulation in the East Sudetes mountain range and constrained the timing of its formation with *in situ*  $^{10}\text{Be}$  surface exposure ages. Our results indicate that the morphology is consistent with that of a block slope produced by bedrock disintegration and downslope movement of resulting blocks. The morphological evidence, block characteristics and chronological data contradict previous interpretations of the landform as a block field or rock glacier. Hence, the palaeoclimatic significance of the landform is limited allowing only for rough approximation of cold conditions in the Sudetes during the past glacial cycles.

Surface exposure ages reveal that the Sut' ridge was transformed under periglacial conditions over several cold periods. The surface exposure age of  $150.1 \pm 4.8$  ka obtained for the tor at the upper limit of the block slope represents the first chronological evidence for the occurrence of permafrost and periglacial activity in the Sudetes during the penultimate (Saalian) cold period. The exposure age estimates retrieved for block samples provide evidence for the formation of the block slope between  $84.3 \pm 3.8$  and  $26.8 \pm 2.6$  ka. Considering the uncertainties of these ages, the emplacement of blocks coincides with warmer stages (MIS 5 and 3) of the Weichselian. The established chronology corresponds with the timing of many block fields and block slopes in

Europe confirming formation of these landforms prior rock glaciers. These findings can stimulate further research of coarse debris accumulations that are widespread throughout the central European uplands and mid-latitude mountain regions.

### Declaration of competing interests

The authors declare that they have no known competing financial interests or personal relationships that could have appeared to influence the work reported in this paper.

### Acknowledgements

This work was supported by the Czech Science Foundation [grant number 17-21612S]. ASTER AMS national facility (CEREGE, Aix-en-Provence) is supported by the INSU/CNRS, the ANR through the "Projets thématiques d'excellence" program for the "Equipements d'excellence" ASTER-CEREGE action, IRD. The Administration of the Protected Landscape Area of Jeseníky is acknowledged for providing permissions to work in the field.

### References

- Agosta, E.A., Compagnucci, R.H., 2016. Abrupt climate changes during the Marine Isotope Stage 3 (MIS 3). In: Gasparini, G., Rabassa, J., Deschamps, C., Tonni, E. (Eds.), *Marine Isotope Stage 3 in Southern South America*, 60 ka B.P.–30 ka B.P. Springer, Cham, pp. 81–106. [https://doi.org/10.1007/978-3-319-40000-6\\_5](https://doi.org/10.1007/978-3-319-40000-6_5)
- Alexandrowicz, W.P., Ciszek, D., Gołas-Siarzewska, M., 2013. Malacological characteristic of the Weichselian Upper Pleniglacial (MIS-2) loess profile in Tłumaczów (SW Poland). *Geol. Q.* 57 (3), 433–442. <https://doi.org/10.7306/gq.1104>
- Andersen, J.L., Egholm, D.L., Knudsen, M.F., Linge, H., Jansen, J.D., Goodfellow, B.W., Pedersen, V.K., Tikhomirov, D., Olsen, J., Fredin, O., 2018. Pleistocene evolution of a Scandinavian plateau landscape. *J. Geophys. Res. Earth Surf.* 123, 3370–3387. <https://doi.org/10.1029/2018JF004670>
- Andrés, N., Gómez-Ortiz, A., Fernández-Fernández, J.M., Tanarro, L.M., Salvador-Franch, F., Oliva, M., Palacios, D., 2018. Timing of deglaciation and rock glacier origin in the southeastern Pyrenees: a review and new data. *Boreas* 47, 1050–1071. <https://doi.org/10.1111/bor.12324>
- Andrieux, E., Bateman, M., Bertran, P., 2018. The chronology of Late Pleistocene thermal contraction cracking derived from sand wedge OSL dating in central and southern France. *Glob. Planet. Chang.* 162, 84–100. <https://doi.org/10.1016/j.gloplacha.2018.01.012>
- Antoine, P., Rousseau, D.-D., Degeai, J.-P., Moine, O., Lagroix, F., Kreutzer, S., Fuchs, M., Hatté, C., Gauthier, C., Svoboda, J., Lisá, L., 2013. High-resolution record of the environmental response to climatic variations during the last interglacial-glacial cycle in Central Europe: the loess-palaeosol sequence of Dolní Věstonice (Czech Republic). *Quat. Sci. Rev.* 67, 17–38. <https://doi.org/10.1016/j.quascirev.2013.01.014>
- Antoine, P., Coutard, S., Guerin, G., Deschodt, L., Goval, E., Lochet, J.-L., Paris, C., 2016. Upper Pleistocene loess-palaeosol records from Northern France in the European context: Environmental background and dating of the Middle Palaeolithic. *Quat. Int.* 411, 4–24. <https://doi.org/10.1016/j.quaint.2015.11.036>
- Arnold, M., Merchel, S., Bourlès, D.L., Braucher, R., Benedetti, L., Finkel, R.C., Aumaître, G., Gottang, A., Klein, M., 2010. The French accelerator mass spectrometry facility ASTER: improved performance and developments. *Nucl. Instr. Meth. B* 268, 1954–1959. <https://doi.org/10.1016/j.nimb.2010.02.107>
- Balco, G., 2020. Glacier change and paleoclimate applications of cosmogenic-nuclide exposure dating. *Annu. Rev. Earth Planet. Sci.* 48, 21–48. <https://doi.org/10.1146/annurev-earth-081619-052609>
- Ballantyne, C.K., 1998. Age and significance of mountain-top detritus. *Permafrost. Periglac. Process.* 9, 327–345. [https://doi.org/10.1002/\(SICI\)1099-1530\(199810/12\)9:4<327::AID-PPP298>3.0.CO;2-9](https://doi.org/10.1002/(SICI)1099-1530(199810/12)9:4<327::AID-PPP298>3.0.CO;2-9)
- Ballantyne, C.K., 2010a. A general model of autochthonous blockfield evolution. *Permafrost. Periglac. Process.* 21, 289–300. <https://doi.org/10.1002/ppp.700>
- Ballantyne, C.K., 2010b. Extent and deglacial chronology of the last British-Irish Ice Sheet: implications of exposure dating using cosmogenic isotopes. *J. Quat. Sci.* 25, 515–534. <https://doi.org/10.1002/jqs.1310>
- Ballantyne, C.K., Stone, J.O., 2015. Trilineas, blockfields and the vertical extent of the last ice sheet in southern Ireland. *Boreas* 44, 277–287. <https://doi.org/10.1111/bor.12109>
- Ballantyne, C.K., Schnabel, C., Xu, S., 2009. Exposure dating and reinterpretation of coarse debris accumulations ('rock glaciers') in the Cairngorm Mountains, Scotland. *J. Quat. Sci.* 24, 19–31. <https://doi.org/10.1002/jqs.1189>
- Barrows, T.T., Stone, J.O., Fifield, L.K., 2004. Exposure ages for Pleistocene periglacial deposits in Australia. *Quat. Sci. Rev.* 23 (5–6), 697–708. <https://doi.org/10.1016/j.quascirev.2003.10.011>
- Bierman, P.R., Thompson Davis, P., Corbett, L.B., Lifton, N.A., Finkel, R.C., 2015. Cold-based Laurentide ice covered New England's highest summits during the Last Glacial Maximum. *Geology* 43 (12), 1059–1062. <https://doi.org/10.1130/G37225.1>
- Blomdin, R., Stroeven, A.P., Harbor, J.M., Lifton, N.A., Heyman, J., Gribenski, N., Petrakov, D. A., Caffee, M.W., Ivanov, M.N., Hättestrand, C., Rogozhina, I., Usabaliyev, R., 2016. Evaluating the timing of former glacier expansions in the Tian Shan: a key step towards robust spatial correlations. *Quat. Sci. Rev.* 153, 78–96. <https://doi.org/10.1016/j.quascirev.2016.07.029>
- Borchers, B., Marrero, S., Balco, G., Caffee, M., Goehring, B., Lifton, N., Nishiizumi, K., Phillips, F., Schaefer, J., Stone, J., 2016. Geological calibration of spallation production rates in the CRONUS-Earth project. *Quat. Geochronol.* 31, 188–198. <https://doi.org/10.1016/j.quageo.2015.01.00>
- Braucher, R., Merchel, S., Borgomano, J., Bourlès, D.L., 2011. Production of cosmogenic radionuclides at great depth: a multi element approach. *Earth Planet. Sci. Lett.* 309 (1–2), 1–9. <https://doi.org/10.1016/j.epsl.2011.06.036>
- Braucher, R., Guillou, V., Bourlès, D.L., Arnold, M., Aumaître, G., Keddadouche, K., Nottoli, E., 2015. Preparation of ASTER in-house <sup>10</sup>Be/<sup>9</sup>Be standard solutions. *Nucl. Instr. Meth. B* 361, 335–340. <https://doi.org/10.1016/j.nimb.2015.06.012>
- Brazier, V., Kirkbride, M., Owens, I., 1998. The relationship between climate and rock glacier distribution in the Ben Ohau Range, New Zealand. *Geogr. Ann.* 80 (3–4), 193–207. <https://doi.org/10.1111/j.0435-3676.1998.00037.x>
- Brook, E.J., Nesje, A., Lehman, S.J., Raisbeck, G.M., Yiou, F., 1996. Cosmogenic nuclide exposure ages along a vertical transect in western Norway – implications for the height of the Fennoscandian ice sheet. *Geology* 24, 207–210. [https://doi.org/10.1130/0091-7613\(1996\)024<0207:CNEAAA>2.3.CO;2](https://doi.org/10.1130/0091-7613(1996)024<0207:CNEAAA>2.3.CO;2)
- Caine, N., Jennings, J., 1968. Some blockstreams of the Toolong Range, Kosciusko State Park, New South Wales. *J. Proc. R. Soc. NSW* 101, 93–103.
- Calderoni, G., Guglielmin, M., Tellini, C., 1998. Radiocarbon dating and postglacial evolution, Upper Valtellina and Livignese area, Sondrio, Central Italian Alps. *Permafrost. Periglac. Process.* 9, 275–284. [https://doi.org/10.1002/\(SICI\)1099-1530\(199807/09\)9:3<275::AID-PPP288>3.0.CO;2-U](https://doi.org/10.1002/(SICI)1099-1530(199807/09)9:3<275::AID-PPP288>3.0.CO;2-U)
- Carr, S.J., Engel, Z., Kalvoda, J., Parker, A., 2002. Sedimentary evidence to suggest extensive glaciation of the Úpa Valley, Krkonoše Mountains, Czech Republic. *Z. Geomorphol.* 46 (4), 523–537. <https://doi.org/10.1127/zfg/46/2002/523>
- Chmal, H., Traczyk, A., 1993. Plejstoceńskie lodowce gruzowe w Karkonoszach. *Czas Geogr.* 64 (3–4), 253–262.
- Chmal, H., Traczyk, A., 1999. Die Vergletscherung des Riesengebirges. *Z. Geomorphol. Suppl.* 113, 11–17.
- Chmieleff, J., von Blanckenburg, F., Kossert, K., Jakob, D., 2010. Determination of the <sup>10</sup>Be half-life by multicollector ICP-MS and liquid scintillation counting. *Nucl. Instr. Meth. B* 268, 192–199. <https://doi.org/10.1016/j.nimb.2009.09.012>
- Çiner, A., Sankaya, M.A., Yıldırım, C., 2017. Misleading old age on a young landform? The dilemma of cosmogenic inheritance in surface exposure dating: Moraines vs. rock glaciers. *Quat. Geochronol.* 42, 76–88. <https://doi.org/10.1016/j.quageo.2017.07.003>
- Clark, P.U., Dyke, A.S., Shakun, J.D., Carlson, A.E., Clark, J., Wohlfarth, B., Mitrovica, J.X., Hostetler, S.W., McCabe, A.M., 2009. The Last Glacial Maximum. *Science* 325 (5941), 710–713. <https://doi.org/10.1126/science.1172873>
- Colleoni, F., Wekerle, C., Näslund, J.O., Brandefelt, J., Masina, S., 2016. Constraint on the penultimate glacial maximum Northern Hemisphere ice topography (≈140 kyrs BP). *Quat. Sci. Rev.* 137, 97–112. <https://doi.org/10.1016/j.quascirev.2016.01.024>
- COSMC, 2016. *Digital Terrain Model of the Czech Republic of the 5th Generation (DMR 5G)*. Czech Office for Surveying, Mapping and Cadastre, Praha.
- Cossart, E., Braucher, R., Fort, M., Bourlès, D.L., Carcaillet, J., 2008. Slope instability in relation to glacial debuitressing in alpine areas (Upper Durance catchment, southeastern France): evidence from field data and <sup>10</sup>Be cosmic ray exposure ages. *Geomorphology* 95 (1–2), 3–26. <https://doi.org/10.1016/j.geomorph.2006.12.022>
- Cremins, D.L., Darmody, R.G., George, S.E., 2005. Upper slope landforms and age of bedrock exposures in the St. Francois Mountains, Missouri: a comparison to relict periglacial features in the Appalachian Plateau of West Virginia. *Geomorphology* 70, 71–84. <https://doi.org/10.1016/j.geomorph.2005.04.001>
- Crest, Y., Delmas, M., Braucher, R., Gunnell, Y., Calvet, M., ASTER Team, 2017. Cirques have growth spurts during deglacial and interglacial periods: evidence from <sup>10</sup>Be and <sup>26</sup>Al nuclide inventories in the central and eastern Pyrenees. *Geomorphology* 278, 60–77. <https://doi.org/10.1016/j.geomorph.2016.10.035>
- Czudek, T., 2005. *Vývoj relief České republiky v kvartéru*. Moravské zemské museum, Brno.
- Daniél, M., Materna, J., Honig, V., Metelka, L., Danielová, V., Harčarik, J., Kliegrová, S., Grubhoffer, L., 2009. Vertical distribution of the tick *Ixodes ricinus* and tick-borne pathogens in the northern Moravian mountains correlated with climate warming (Jeseniky Mts., Czech Republic). *Cent. Eur. J. Public Health* 17 (3), 139–145. <https://doi.org/10.21101/cejpha.3550>
- Danišík, M., Migoń, P., Kuhlemann, J., Evans, N.J., Dunkl, I., Frisch, W., 2010. Thermochronological constraints on the long-term erosional history of the Karkonosze Mts., Central Europe. *Geomorphology* 117, 78–89. <https://doi.org/10.1016/j.geomorph.2009.11.010>
- Dede, V., Çiçek, I., Sankaya, M.A., Çiner, A., Uncu, L., 2017. First cosmogenic geochronology from the Lesser Caucasus: Late Pleistocene glaciation and rock glacier development in the Karçal Valley, NE Turkey. *Quat. Sci. Rev.* 164, 54–67. <https://doi.org/10.1016/j.quascirev.2017.03.025>
- Del Vecchio, J., DiBiase, R.A., Denn, R.A., Bierman, P.R., Caffee, M.W., Zimmerman, S.R., 2018. Record of coupled hillslope and channel response to Pleistocene erosion and deposition in a sandstone headwater valley, Central Pennsylvania. *GSA Bull.* 130 (11–12), 1903–1917. <https://doi.org/10.1130/B31912.1>
- Denn, A.R., Bierman, P.R., Zimmerman, S.R.H., Caffee, M.W., Corbett, L.B., Kirby, E., 2018. Cosmogenic nuclides indicate that boulder fields are dynamic, ancient, multigenerational features. *GSA Today* 28, 4–10. <https://doi.org/10.1130/GSATG340A.1>
- Dunne, J., Elmore, D., Muzikar, P., 1999. Scaling factors for the rates of production of cosmogenic nuclides for geometric shielding and attenuation at depth on sloped surfaces. *Geomorphology* 27, 3–11. [https://doi.org/10.1016/S0169-555X\(98\)00086-5](https://doi.org/10.1016/S0169-555X(98)00086-5)
- Ehlers, J., Gibbard, P.L., Hughes, P.D. (Eds.), 2011. *Quaternary Glaciations – Extent and Chronology: A Closer Look*. Elsevier, Amsterdam.

- Engel, Z., 2007. Measurement and age assignment of intact rock strength in the Krkonoše Mountains, Czech Republic. *Z. Geomorphol.* 51 (Suppl. 1), 69–80. <https://doi.org/10.1127/0372-8854/2007/00515-0069>.
- Engel, Z., Braucher, R., Traczyk, A., Leanni, L., ASTER Team, 2014. <sup>10</sup>Be exposure age chronology of the last glaciation in the Krkonoše Mountains, Central Europe. *Geomorphology* 206, 107–121. <https://doi.org/10.1016/j.geomorph.2013.10.003>.
- Engel, Z., Mentlík, P., Braucher, R., Křížek, M., Pluhačková, M., Aster Team, 2017. <sup>10</sup>Be exposure age chronology of the last glaciation in the Western Tatra Mountains, Central Europe. *Geomorphology* 293, 130–142. <https://doi.org/10.1016/j.geomorph.2017.05.012>.
- Fernández-Fernández, J.M., Palacios, D., García-Ruiz, J.M., Andrés, N., Schimmelpfennig, I., Gómez-Villar, A., Santos-González, J., Álvarez-Martínez, J., Arnáez, J., Úbeda, J., Léanni, L., Aumaitre, G., Bourlès, D., Keddadouche, K., 2017. Chronological and geomorphological investigation of fossil debris-covered glaciers in relation to deglaciation processes: a case study in the Sierra de La Demanda, northern Spain. *Quat. Sci. Rev.* 170, 232–249. doi:<https://doi.org/10.1016/j.quascirev.2017.06.034>.
- Feurdean, A., Perşoiu, A., Tanţau, I., Stevens, T., Magyar, E.K., Onac, B.P., Marković, S., Andrić, M., Connor, S., Fărcaş, S., Gaik, M., Gaudenyi, T., Hoek, W., Kolaczek, P., Kuneš, P., Lamentowicz, M., Marinova, E., Michczyńska, D.J., Perşoiu, I., Plóciennik, M., Słowiński, Stancikaitė, M., Sumegi, P., Svensson, A., Tamaş, T., Timar, A., Tonkov, S., Toth, M., Veski, S., Willis, K.J., Zernitskaya, V., 2014. Climate variability and associated vegetation response throughout Central and Eastern Europe (CEE) between 60 and 8 ka. *Quat. Sci. Rev.* 106, 206–224. doi:<https://doi.org/10.1016/j.quascirev.2014.06.003>.
- Fuchs, M.C., Böhlert, R., Krbetschek, M., Preusser, F., Egli, M., 2013. Exploring the potential of luminescence methods for dating Alpine rock glaciers. *Quat. Geochronol.* 18, 17–33. <https://doi.org/10.1016/j.quageo.2013.07.001>.
- Goodfellow, B.W., 2007. Relict non-glacial surfaces in formerly glaciated landscapes. *Earth-Sci. Rev.* 80, 47–73. <https://doi.org/10.1016/j.earscirev.2006.08.002>.
- Goodfellow, B.W., Stroeven, A.P., Fabel, D., Fredin, O., Derron, M., Bintanja, R., Caffee, M., 2014. Arctic-alpine blockfields in the northern Swedish Scandes: Late Quaternary – not Neogene. *Earth Surf. Dyn.* 2 (2), 383–401. <https://doi.org/10.5194/esurf-2-383-2014>.
- Gosse, J.C., Phillips, F.M., 2001. Terrestrial *in situ* cosmogenic nuclides: theory and application. *Quat. Sci. Rev.* 20, 1475–1560. [https://doi.org/10.1016/S0277-3791\(00\)00171-2](https://doi.org/10.1016/S0277-3791(00)00171-2).
- Graham, D., Midgley, N., 2000. Graphical representation of particle shape using triangular diagrams: an Excel spreadsheet method. *Earth Surf. Process. Landf.* 25, 1473–1477. [https://doi.org/10.1002/1096-9837\(200012\)25:133.0.CO;2-C](https://doi.org/10.1002/1096-9837(200012)25:133.0.CO;2-C).
- Gualtieri, L., Brigham-Grette, J., 2001. The age and origin of the Little Diomede Island upland surface. *Arctic* 54 (1), 12–21. <https://doi.org/10.14430/arctic759>.
- Gunnell, Y., Jarman, D., Braucher, R., Calvet, M., Delmas, M., Leanni, I., Bourles, D., Arnold, M., Aumaitre, G., Keddadouche, K., 2013. The granite tors of Dartmoor, Southwest England: rapid and recent emergence revealed by Late Pleistocene cosmogenic apparent exposure ages. *Quat. Sci. Rev.* 61, 62–76. <https://doi.org/10.1016/j.quascirev.2012.11.005>.
- Haeblerli, W., Käab, A., Wagner, S., Mühl, D.V., Geissler, P., Haas, J.N., Glatzel-Mattheier, H., Wagenbach, D., 1999. Pollen analysis and <sup>14</sup>C age of moss in a permafrost core recovered from the active rock glacier Murtel-Corvatsch, Swiss Alps: geomorphological and glaciological implications. *J. Glaciol.* 45 (149), 1–8. <https://doi.org/10.1017/S002214300002975>.
- Haeblerli, W., Brandová, D., Burga, C., Egli, M., Frauenfelder, R., Käab, A., Maisch, M., 2003. Methods for absolute and relative age dating of rock-glacier surfaces in alpine permafrost. In: Phillips, M., Springman, S., Arenson, L. (Eds.), *Proceedings of the 8th International Conference on Permafrost 2003*. Zurich. Swets & Zeitlinger, Lisse, pp. 343–348.
- Haeblerli, W., Hallet, B., Arenson, L., Elconin, R., Humlum, O., Käab, A., Kaufmann, V., Ladanyi, B., Matsuoka, N., Springman, S., Mühl, D.V., 2006. Permafrost creep and rock glacier dynamics. *Permafr. Periglac. Process.* 17, 189–214. <https://doi.org/10.1002/ppp.561>.
- Hansom, J.D., Evans, D.J.A., Sanderson, D.C.W., Bingham, R.G., Bentley, M.J., 2008. Constraining the age and formation of stone runs in the Falkland Islands using optically stimulated luminescence. *Geomorphology* 94 (1–2), 117–130. <https://doi.org/10.1016/j.geomorph.2007.05.006>.
- Harris, S.A., 1994. Climatic zonation of periglacial landforms in mountain areas. *Arctic* 47 (2), 184–192. <https://doi.org/10.14430/arctic1288>.
- Heimsath, A.M., Chappell, J., Fifield, K., 2010. Eroding Australia: rates and processes from Bega Valley to Arnhem Land. In: Bishop, P., Pillans, B. (Eds.), *Australian Landscapes*. Geological Society, London, pp. 225–241. <https://doi.org/10.1144/SP346.12>.
- Heiri, O., Koinig, K.A., Spötl, C., Barrett, S., Brauer, A., Drescher-Schneider, R., Gaar, D., Ivy-Ochs, S., Kerschner, H., Luetscher, M., Moran, A., Nicolussi, K., Preusser, F., Schmidt, R., Schoeneich, P., Schwörer, C., Sprafke, T., Terhorst, B., Tinner, W., 2014. Palaeoclimate records 60–8 ka in the Austrian and Swiss Alps and their forelands. *Quat. Sci. Rev.* 106, 186–205. <https://doi.org/10.1016/j.quascirev.2014.05.021>.
- Hopkinson, C., Ballantyne, C.K., 2014. Age and origin of blockfields on Scottish mountains. *Scott. Geogr. J.* 130 (2), 116–141. <https://doi.org/10.1080/14702541.2013.855808>.
- Humlum, O., 1988. Rock glacier appearance level and rock glacier initiation line altitude: a methodological approach to the study of rock glaciers. *Arct. Alp. Res.* 20 (2), 160–178. <https://doi.org/10.1080/0040851.1988.12002662>.
- Janke, J.R., Regmi, N.R., Giardino, J.R., Vitek, J.D., 2013. Rock glaciers. In: Shroder, J., Giardino, R., Harbor, J. (Eds.), *Treatise on Geomorphology*. Academic Press, San Diego, pp. 238–273. <https://doi.org/10.1016/B978-0-12-374739-6.00211-6>.
- Janoušek, V., Aichler, J., Hanžl, P., Gerdes, A., Erban, V., Žáček, V., Pecina, V., Pudilová, M., Hrdličková, K., Míxa, P., Žáčková, E., 2014. Constraining genesis and geotectonic setting of metavolcanic complexes: a multidisciplinary study of the Devonian Vrbno Group (Hrubý Jeseník Mts., Czech Republic). *Int. J. Earth Sci.* 103, 455–483. <https://doi.org/10.1007/s00531-013-0975-4>.
- Knight, J., Harrison, S., Jones, D.B., 2019. Rock glaciers and the geomorphological evolution of deglaciating mountains. *Geomorphology* 324, 14–24. <https://doi.org/10.1016/j.geomorph.2018.09.020>.
- Konrad, S.K., Humphrey, N.F., Steig, E.J., Clark, D.H., Potter, N., Pfeffer, W.T., 1999. Rock glacier dynamics and paleoclimatic implications. *Geology* 27 (12), 1131–1134. [https://doi.org/10.1130/0091-7613\(1999\)027<1131:RGDAP>2.3.CO;2](https://doi.org/10.1130/0091-7613(1999)027<1131:RGDAP>2.3.CO;2).
- Korschinek, G., Bergmaier, A., Faestermann, T., Gerstmann, U.C., Knie, K., Rugel, G., Wallner, A., Dillmann, I., Dollinger, G., Lierse von Gostomski, Ch., Kossert, K., Maiti, M., Poutivtsev, M., Remmert, A., 2010. A new value for the half-life of <sup>10</sup>Be by heavy-ion elastic recoil detection and liquid scintillation counting. *Nucl. Instr. Meth.* B 268, 187–191. doi:<https://doi.org/10.1016/j.nimb.2009.09.020>.
- Krainer, K., Bressan, D., Dietre, B., Haas, J., Hajdas, I., Lang, K., Mair, V., Nickus, U., Reidl, D., Thies, H., Tonidandel, D., 2015. A 10,300-year-old permafrost core from the active rock glacier Lazaun, southern Ötztal Alps (South Tyrol, northern Italy). *Quat. Res.* 83 (2), 324–335. <https://doi.org/10.1016/j.yqres.2014.12.005>.
- Křížek, M., 2016. Periglacial landforms of the Hrubý Jeseník Mountains. In: Pánek, T., Hradecký, J. (Eds.), *Landscapes and Landforms of the Czech Republic*. Springer, Cham, pp. 277–289. <https://doi.org/10.1007/978-3-319-27537-6>.
- Lal, D., 1991. Cosmic ray labeling of erosion surfaces: *in situ* nuclide production rates and erosion models. *Earth Planet. Sci. Lett.* 104, 424–439. [https://doi.org/10.1016/0012-821X\(91\)90220-C](https://doi.org/10.1016/0012-821X(91)90220-C).
- Lehmkuhl, F., Zens, J., Krauß, L., Schulte, P., Kels, H., 2016. Loess-paleosol sequences at the northern European loess belt in Germany: distribution, geomorphology and stratigraphy. *Quat. Sci. Rev.* 153, 11–30. <https://doi.org/10.1016/j.quascirev.2016.10.008>.
- Leśniewicz, S., 1996. Morfologia peryglacialna północnych stoków Łąbskiego Szczytu w Karkonoszach. *Acta Univ. Wratisl. Prace Inst. Geogr.* 1808 (A8), 81–91.
- Lisiecki, L.E., Raymo, M.E., 2005. A Pliocene-Pleistocene stack of 57 globally distributed benthic  $\delta^{18}O$  records. *Paleoceanography* 20, PA 1003. <https://doi.org/10.1029/2004PA001071>.
- Marks, L., Makos, M., Szymanek, M., Woronko, B., Dzierżek, J., Majecka, A., 2019. Late Pleistocene climate of Poland in the mid-European context. *Quat. Int.* 504, 24–39. <https://doi.org/10.1016/j.quaint.2018.01.024>.
- Marquette, G.C., Gray, J.T., Gosse, J.C., Courchesne, F., Stockli, L., Macpherson, G., Finkel, R., 2004. Felsenmeer persistence under non-erosive ice in the Torngat and Kaumajet mountains, Quebec and Labrador, as determined by soil weathering and cosmogenic nuclide exposure dating. *Can. J. Earth Sci.* 41, 19–38. <https://doi.org/10.1139/E03-072>.
- Matsuoka, N., 2001. Solifluction rates, processes and landforms: a global review. *Earth-Sci. Rev.* 55, 107–134. [https://doi.org/10.1016/S0012-8252\(01\)00057-5](https://doi.org/10.1016/S0012-8252(01)00057-5).
- Migoń, P., 1996. Evolution of granite landscapes in the Sudetes (Central Europe): some problems of interpretation. *Proc. Geol. Assoc.* 107, 25–37. [https://doi.org/10.1016/S0016-7878\(96\)80065-4](https://doi.org/10.1016/S0016-7878(96)80065-4).
- Moran, A.P., Ivy Ochs, S., Vockenhuber, C., Kerschner, H., 2016. Rock glacier development in the Northern Calcareous Alps at the Pleistocene-Holocene boundary. *Geomorphology* 273, 178–188. <https://doi.org/10.1016/j.geomorph.2016.08.017>.
- Moseley, G.E., Spötl, C., Svensson, A., Cheng, H., Brandstätter, S., Edwards, R.L., 2014. Multi-speleothem record reveals tightly coupled climate between Central Europe and Greenland during Marine Isotope Stage 3. *Geology* 42, 1043–1046. <https://doi.org/10.1130/G36063.1>.
- Oh, J.J., Park, S.P., Seong, Y.B., 2012. Spatial pattern and surface exposure ages of cryoplanation surface at Mt. Moodeung. [in Korean with English abstract.]. *J. Korean Geomorphol. Assoc.* 19, 83–97.
- Palacios, D., Andrés, N., Marcos, J., Vázquez-Selem, L., 2012. Glacial landforms and their paleoclimatic significance in Sierra de Guadarrama, Central Iberian Peninsula. *Geomorphology* 139–140, 67–78. <https://doi.org/10.1016/j.geomorph.2011.10.003>.
- Palacios, D., Gómez-Ortiz, A., Andrés, N., Vázquez-Selem, L., Salvador-Franch, F., Oliva, M., 2015a. Maximum extent of Late Pleistocene glaciers and last deglaciation of La Cerdanya Mountains, southeastern Pyrenees. *Geomorphology* 231, 116–129. <https://doi.org/10.1016/j.geomorph.2014.10.037>.
- Palacios, D., Gómez-Ortiz, A., Andrés, N., Salvador-Franch, F., Oliva, M., 2016. Timing and new geomorphological evidence of the last deglaciation stages in Sierra Nevada (southern Spain). *Quat. Sci. Rev.* 150, 110–129. <https://doi.org/10.1016/j.quascirev.2016.08.012>.
- Palacios, D., Andrés, N., García-Ruiz, J.M., Schimmelpfennig, I., Campos, N., Léanni, L., Team, Aster, 2017. Deglaciation in the Central Pyrenees during the Pleistocene-Holocene transition: timing and geomorphological significance. *Quat. Sci. Rev.* 150, 110–129. <https://doi.org/10.1016/j.quascirev.2017.03.007>.
- Petránek, J., 1953. *Skalní ledovec u Malé Morávky v Hrubém Jeseníku*. Přírodovědecký sborník Ostravského kraje 14, 1–19.
- Portenga, E.W., Bierman, P.R., Rizzo, D.M., Root, D.H., 2013. Low rates of bedrock outcrop erosion in the central Appalachian Mountains inferred from *in situ* <sup>10</sup>Be. *GSA Bull.* 125 (1–2), 201–215. <https://doi.org/10.1130/B30559.1>.
- Railsback, L.B., Gibbard, P.L., Head, M.J., Voarintsoa, N.R.G., Toucanne, S., 2015. An optimized scheme of lettered marine isotope substages for the last 1.0 million years, and the climatostratigraphic nature of isotope stages and substages. *Quat. Sci. Rev.* 111, 94–106. <https://doi.org/10.1016/j.quascirev.2015.01.012>.
- Rasmussen, S.O., Bigler, M., Blockley, S., Blunier, T., Buchardt, S.L., Clausen, H.B., Cvijanovic, I., Dahl-Jensen, D., Johnsen, S.J., Fischer, H., Gkinis, V., Guillevic, M., Hoek, W.Z., Lowe, J.J., Pedro, J.B., Popp, T., Seierstad, I.K., Steffensen, J.P., Svensson, A.M., Vallenga, P., Vinther, B.M., Walker, M.J.C., Wheatley, J.J., Winstrup, M., 2014. A stratigraphic framework for abrupt climatic changes during the Last Glacial period based on three synchronized Greenland ice-core records: refining and extending the INTIMATE event stratigraphy. *Quat. Sci. Rev.* 106, 14–28. <https://doi.org/10.1016/j.quascirev.2014.09.007>.
- Rea, B., 2013. Blockfields (Felsenmeer). In: Elias, S.A. (Ed.), *Encyclopedia of Quaternary Science*. Elsevier, Amsterdam, pp. 523–534. <https://doi.org/10.1016/B978-0-444-53643-3.00103-5>.

- Rhee, H.-H., Seong, Y.-B., Jeon, Y.-G., Yu, B.-Y., 2017. Bouldery slope landforms on Mt. Biseul, Korea, and implications for paleoclimate and slope evolution. *Quat. Res.* 88, 293–312. <https://doi.org/10.1017/qua.2017.27>.
- Rixhon, G., Demoulin, A., 2013. Evolution of slopes in a cold climate. In: Shroder, J., Giardino, R., Harbor, J. (Eds.), *Treatise on Geomorphology*. Academic Press, San Diego, pp. 392–415. <https://doi.org/10.1016/B978-0-12-374739-6.00218-9>.
- Rodríguez-Rodríguez, L., Jiménez-Sánchez, M., Domínguez-Cuesta, M.J., Rinterknecht, V., Pallàs, R., Bourlès, D., 2016. Chronology of glaciations in the Cantabrian Mountains (NW Iberia) during the last Glacial Cycle based on *in situ*-produced  $^{10}\text{Be}$ . *Quat. Sci. Rev.* 138, 31–48. <https://doi.org/10.1016/j.quascirev.2016.02.027>.
- Rodríguez-Rodríguez, L., Jiménez-Sánchez, M., Domínguez-Cuesta, M.J., Rinterknecht, V., Pallàs, R., Team, Aster, 2017. Timing of last deglaciation in the Cantabrian Mountains (Iberian Peninsula; North Atlantic region) based on *in situ*-produced  $^{10}\text{Be}$  exposure dating. *Quat. Sci. Rev.* 171, 166–181. <https://doi.org/10.1016/j.quascirev.2017.07.012>.
- Scapozza, C., Lambiel, C., Reynard, E., Fallot, J.-M., Antognini, M., Schoeneich, P., 2010. Radiocarbon dating of fossil wood remains buried by the Piancabella rock glacier, Blenio Valley (Ticino, southern Swiss Alps): implications for rock glacier, treeline and climate history. *Permafrost. Periglac. Process.* 21, 90–96. <https://doi.org/10.1002/ppp.673>.
- Seguinot, J., Jouvét, G., Huss, M., Funk, M., Ivy-Ochs, S., Preusser, F., 2018. Modelling last glacial cycle ice dynamics in the Alps. *Cryosphere* 12, 3265–3285. <https://doi.org/10.5194/tc-12-3265-2018>.
- Sekyra, J., Sekyra, Z., 2002. Former existence of a plateau icefield in Bilá Louka meadow, eastern Giant Mountains: hypothesis and evidence. *Opera Corcon.* 39, 39–43.
- Seong, Y.B., Kim, J.W., 2003. Application of *in situ* produced cosmogenic  $^{10}\text{Be}$  and  $^{26}\text{Al}$  for estimating erosion rate and exposure age of tor and block stream detritus: case study from Mt. Maneo, South Korea. *J. Korean Geogr. Soc.* 38 (3), 389–399.
- Shakesby, R.A., Dawson, A.G., Matthews, J.A., 1987. Rock glaciers, protalus ramparts and related phenomena, Rondane, Norway: a continuum of large-scale talus-derived landforms. *Boreas* 16, 305–317. <https://doi.org/10.1111/j.1502-3885.1987.tb00099.x>.
- Skrzypiek, G., Wiśniewski, A., Grierson, P.F., 2011. How cold was it for Neanderthals moving to Central Europe during warm phases of the last glaciation? *Quat. Sci. Rev.* 30, 481–487. <https://doi.org/10.1016/j.quascirev.2010.12.018>.
- Sobíšek, B., 2000. Rychlost a směr větru na území České republiky v období 1961–1990. *Český hydrometeorologický ústav, Praha*.
- van Steijn, H., Boelhouwers, J., Harris, S., Héty, B., 2002. Recent research on the nature, origin and climatic relations of blocky and stratified slope deposits. *Prog. Phys. Geogr.* 26 (4), 551–575. <https://doi.org/10.1191/0309133302pp352ra>.
- Stone, J.O., 2000. Air pressure and cosmogenic isotope production. *J. Geophys. Res.* 105, 23753–23759. <https://doi.org/10.1029/2000JB900181>.
- Svendsen, J., Alexanderson, H., Astakhov, V., Demidov, I., Julian, A., Funder, S., Gataulling, V., Henriksen, M., Hjort, J., Houmark-Nielsen, M., Hubberten, H., Ingulfsson, O., Jakobsson, M., Kjer, K., Larsen, E., Lokrantz, H., Lunkka, J., Lys, A., Mangerud, J., Matiouchkov, A., Murray, A., Muller, P., Niessen, F., Nikolskaya, O., Polyak, L., Saamisto, M., Siegert, C., Siegert, M., Spielhagen, R., Ruedige, S., 2004. Late Quaternary ice sheet history of Northern Eurasia. *Quat. Sci. Rev.* 23, 1229–1271. <https://doi.org/10.1016/j.quascirev.2003.12.008>.
- Traczyk, A., 1996. Geneza i znaczenie stratygraficzne rytmicznie warstwowanych osadów stokowych w Sudetach. *Acta Univ. Wratisl. Prace Inst. Geogr.* 8, 93–104.
- Traczyk, A., 2004. Late Pleistocene evolution of periglacial and glacial relief in the Karkonosze Mountains. New hypotheses and research perspectives. *Acta Univ. Carol. Geogr.* 39, 59–72.
- Traczyk, A., Migoń, P., 2000. Cold-climate landform patterns in the Sudetes. Effect of lithology, relief and glacial history. *Acta Univ. Carol. Geogr. Suppl.* 35, 185–210.
- Traczyk, A., Żurawek, R., 1999. Pleistozäne Schuttdecken und Schuttlagen im nordwestlichen Teil des Ślęża-Massivs (Polen) und ihre Entstehung unter den Bedingungen eines Dauerfrostbodens. *Petermanns Geogr. Mitt.* 143, 131–141.
- Treml, V., Migoń, P., 2015. Controlling factors limiting timberline position and shifts in the Sudetes: a review. *Geogr. Pol.* 88, 55–70. <https://doi.org/10.7163/GPol.0015>.
- Uxa, T., Krížek, M., Krause, D., Hartvich, F., Tábořík, P., Kasprzak, M., 2019. Comment on “Geophysical approach to the study of a periglacial blockfield in a mountain area (Ztracené kameny, Eastern Sudetes, Czech Republic)” by Stan et al. (2017). *Geomorphology* 328, 231–237. <https://doi.org/10.1016/j.geomorph.2018.10.010>.
- Van Meerbeeck, C.J., Renssen, H., Roche, D.M., Wolfarth, B., Bohncke, S.J.P., Bos, J.A.A., Engels, S., Helmens, K.F., Sánchez-Goni, M.F., Svensson, A., Vandenberghe, J., 2011. The nature of MIS 3 stadial–interstadial transitions in Europe: new insights from model–data comparisons. *Quat. Sci. Rev.* 30, 3618–3637. <https://doi.org/10.1016/j.quascirev.2011.08.002>.
- Wilson, P., 2013. Block/rock streams. In: Elias, S.A. (Ed.), *Encyclopedia of Quaternary Science*. Elsevier, Amsterdam, pp. 514–522. <https://doi.org/10.1016/B978-0-444-53643-3.00102-3>.
- Wilson, P., Bentley, M.J., Schnabel, C., Clark, R., Xu, S., 2008. Stone run (block stream) formation in the Falkland Islands over several cold stages, deduced from cosmogenic isotope ( $^{10}\text{Be}$  and  $^{26}\text{Al}$ ) surface exposure dating. *J. Quat. Sci.* 23 (5), 461–473. <https://doi.org/10.1002/jqs.1156>.
- Wilson, P., Matthews, J.A., Mourné, R.W., 2017. Relict blockstreams at Insteheia, Valldalen-Tafjorden, southern Norway: their nature and Schmidt Hammer exposure age. *Permafrost. Periglac. Process.* 28, 286–297. <https://doi.org/10.1002/ppp.1915>.
- Woronko, B., Zieliński, P., Sokołowski, R.J., 2015. Climate evolution during the Pleniglacial and Late Glacial as recorded in quartz grain morphoscopy of fluvial to aeolian successions of the European Sand Belt. *Geologos* 21, 89–103. <https://doi.org/10.1515/logos-2015-0005>.
- Žák, K., Richter, D.K., Filippi, M., Živor, R., Deininger, M., Mangini, A., Scholz, D., 2012. Coarsely crystalline cryogenic cave carbonate – a new archive to estimate the Last Glacial Minimum permafrost depth in Central Europe. *Clim. Past* 8, 1821–1837. <https://doi.org/10.5194/cp-8-1821-2012>.
- Zasadni, J., Kłapyta, P., Broś, E., Ivy-Ochs, S., Świąder, A., Christl, M., Balážovičová, L., 2020. Latest Pleistocene glacier advances and post-Younger Dryas rock glacier stabilization in the Mt. Kriváň group, High Tatra Mountains, Slovakia. *Geomorphology* 358, 107093. <https://doi.org/10.1016/j.geomorph.2020.107093>.
- Żurawek, R., 1999. Relict rock glaciers in the central European Mid-Mountains. *State-of-the-art. Biul. Periglac.* 38, 163–192.
- Żurawek, R., Migoń, P., 1999. Peryglacialna morfogeneza Ślęży w kontekście długotrwałej ewolucji rzeźby. *Acta Geogr. Lodz* 76, 133–155.